Nanoscale

PAPER

View Article Online
View Journal | View Issue

Cite this: *Nanoscale*, 2015, **7**, 559

Published on 10 November 2014. Downloaded by Fail Open on 23/07/2025 9:15:02 AM.

Flexible 3D porous CuO nanowire arrays for enzymeless glucose sensing: *in situ* engineered *versus ex situ* piled†

Jianfei Huang, Yihua Zhu,* Xiaoling Yang, Wei Chen, Ying Zhou and Chunzhong Li*

Received 25th September 2014,
Accepted 5th November 2014

DOI: 10.1039/c4nr05620e

www.rsc.org/nanoscale

Convenient determination of glucose in a sensitive, reliable and cost-effective way has aroused sustained research passion, bringing along assiduous investigation of high-performance electroactive nanomaterials to build enzymeless sensors. In addition to the intrinsic electrocatalytic capability of the sensing materials, electrode architecture at the microscale is also crucial for fully enhancing the performance. In this work, free-standing porous CuO nanowire (NW) was taken as a model sensing material to illustrate this point, where an *in situ* formed 3D CuO nanowire array (NWA) and CuO nanowires pile (NWP) immobilized with polymer binder by conventional drop-casting technique were both studied for enzymeless glucose sensing. The NWA electrode exhibited greatly promoted electrochemistry characterized by decreased overpotential for electro-oxidation of glucose and over 5-fold higher sensitivity compared to the NWP counterpart, benefiting from the binder-free nanoarray structure. Besides, its sensing performance was also satisfying in terms of rapidness, selectivity and durability. Further, the CuO NWA was utilized to fabricate a flexible sensor which showed excellent performance stability against mechanical bending. Thanks to its favorable electrode architecture, the CuO NWA is believed to offer opportunities for building high-efficiency flexible electrochemical devices.

Introduction

Realizing sensitive, rapid and convenient detection of glucose is highly desirable for a range of occasions including fundamental biological research, bioengineering applications, food industries, and diagnosis/monitoring of diabetes, for which enzyme-involved biosensors have been extensively explored due to the highly selective bio-redox interaction between the enzymes and glucose.[1,2] Nevertheless, high cost, limited durability, critical operational conditions, complicated electrode construction and challenges in direct electron transfer have cast a shadow over them.[3,4] In this context, passionate endeavor has been dedicated to exploring enzymeless electrochemical platforms for glucose sensing.[5,6] Excellent in electrocatalysis as they are, noble metals and their alloys are not economical for large-scale manufacturing considering the prohibitive price and the scarcity of the raw materials. Vulnerability to chloride ion (Cl^-) poisoning also seriously degrades their utility.[3,7,8] Currently, non-precious transition metals and metal oxides are drawing increasing attention as cost-effective alternatives. Cupric oxide (CuO) was shown to be an attractive earth-abundant transition metal oxide for building enzymeless platforms for electrochemical detection.[5,6,8,9] In addition to rational selection of candidate electroactive materials, performance enhancement has also been enabled by downsizing the electrode materials. Fruitful results in electrochemical fields including chemical sensing,[10] fuel cells,[11] (photo)electrochemical water splitting,[12,13] Li-ion batteries[14] and supercapacitors[15] have vividly instantiated promoted electrode kinetics and performance upgrade enabled by nanoscaling the electrode materials that provides massively enlarged surface areas and mass transport resistance.[16,17] Particularly, one-dimensional (1D) nanostructures (wire, tube, rod and belt) incorporating defined charge transport pathways and abundant surface areas have gained considerable research popularity in microelectronics and electrochemistry, holding exciting promise for building the next generation of nanoelectronics

---

Key Laboratory for Ultrafine Materials of Ministry of Education, School of Materials Science and Engineering, East China University of Science and Technology, Shanghai 200237, China. E-mail: yhzhu@ecust.edu.cn, czli@ecust.edu.cn; Fax: +86 21 6425 0624; Tel: +86 21 6425 2022

† Electronic supplementary information (ESI) available: TEM images of CuO nanowires. SEM images of the composite film of CuO NWs in the Nafion binder. Flowchart of electrodes fabrication procedures. Current response time to addition of the glucose. Amperometric *i–t* test for the NWP under +0.35 V. Nyquist plot of the electrodes. SEM images of fractured parts of CuO nanowires at the NWP-Nafion film. Parameter comparison of enzymeless sensors for glucose detection. See DOI: 10.1039/c4nr05620e

Published on 10 November 2014. Downloaded by Fail Open on 23/07/2025 9:15:02 AM.

and electrochemical devices.[10,13–16,18–21] In this work, we thereby sought to exploit 1D CuO NW as the electrode material for enzymeless glucose sensing.

Micro-/nano-scale morphologies of electrocatalysts have received huge attention as decisive factors in their performance.[22,23] However, less emphasis has been placed on the influence of electrode architecture at the level between nanosized electrocatalytic units and macroscopic electrodes, which calls for more attention if the electrocatalytic potential is to be fully realized. Consider the case of 1D nanomaterials, vertically aligned array structure[10,16,24,25] and disorderly piled-up nanowires,[26–29] which are the two most common electrode architectures for present amperometric sensors. An issue arousing concerns for the latter is that they typically require the assistance of co-casted polymer binders such as Nafion, polyvinylidene fluoride (PVDF) or chitosan to form a matrix film within which the active substances can be immobilized and connected to the current collector. The negative effects of the employment of binders have been widely ascribed to the strong diffusion resistance and inevitable circumstance of partial blocking/burying of the electroactive materials.[16,30–32] Moreover, the polymer binders usually make no contribution to catalysing the reactions themselves, have poor conductivity, and introduce additional costs and technical manipulations. To circumvent this, synthetic strategies as well as overall electrode design should be considered to realize *in situ* nanowire structure. A well-aligned vertical array of CuO NWs can be developed by the hot plate method,[33] which was based on to fabricate functional electrodes.[16,34,35] Unfortunately, scaling-up of this method is hindered by the high temperature and long annealing duration required. It also often causes serious oxidation in thin foil substrate, which may suffer from deformation and embrittlement,[16] making further device assembly difficult. Therefore, it is necessary to design another route that avoids these unwanted consequences.

With the above motivations, we herein present the *in situ* synthesis of a vertical porous CuO nanowire array (NWA) on a conductive substrate *via* a conversion strategy. The as-prepared CuO NWA was then applied to enzymelessly detect glucose with high sensitivity, reliable stability and eligible selectivity, and its superiority over binder co-casted CuO NWs modified electrode was studied. Furthermore, thanks to the moderate temperature in the preparation process, the thin foil as the supporting substrate of CuO NWA remained metallic without being totally oxidized into crispy copper oxides, allowing further integration with polyethylene terephthalate (PET) to obtain an archetypal flexible sensor that gave stable amperometric signal feedback under and after mechanical bending.

Results and discussion

Materials synthesis and characterizations

Ambient dry oxidation of copper substrates has been found to produce large-area vertical CuO NWs. Despite its one-step directness and facility over template-mediated methods, this approach requires a temperature up to 400–500 °C and relatively long heating duration,[33,34] which is rather energy-intensive, time-consuming, and renders thin substrates mechanically fragile and poorly conductive. Hence, an alternative route towards a high-density array of CuO NW was adopted in the present work, which utilized solution-processed $Cu(OH)_2$ NWA as the precursor.[36] The preparation route is illustrated in Fig. 1a1. A copper foil was subject to an alkaline oxidative etchant solution (AOES) containing $(NH_4)_2S_2O_8$ and NaOH to generate $Cu(OH)_2$ NWA at room temperature, followed by thermal treatment at a much lower temperature (180 °C) for simultaneous dehydration of $Cu(OH)_2$ and improved crystallization of CuO,[37] giving the final product of CuO NWA. Successful realization of the synthetic route was initially indicated by the stepwise color changes of the starting foil from the bright orange typical of metallic Cu to the blue of the intermediate $Cu(OH)_2$ NWA and eventually dark brown of the target product CuO NWA, which are shown in Fig. 1a2. Moreover, it can be seen that the cut edge of the CuO NWA foil has a metallic lustre, visually suggesting limited oxidation into the thickness of the thin foil substrate.

Component identification was conducted using X-ray diffraction (XRD). The XRD patterns in Fig. 1b1 and b2 are for the foils covered with $Cu(OH)_2$ and CuO NWAs, respectively. For the former, diffraction peaks at 16.6°, 23.7°, 34°, 35.8°, 38.1°, 39.7° and 53.3° are clearly discernible, corresponding well to the (020), (021), (002), (111), (022), (130), and (150) planes of orthorhombic structured $Cu(OH)_2$. Note that the three strong diffraction peaks at 43.3°, 50.4° and 74.3° corresponding to the cubic structure of metallic copper are from the Cu substrate. However, the latter one only gives two faintly recognizable peaks at 35.5° and 38.8° characteristic of the (−111) and (111) planes of the monoclinic CuO. This moderate signal is possibly due to the strong signals from the underlying Cu substrate and the small size of the CuO crystalline grain. Therefore, scratched CuO NW powders were also studied, whose XRD pattern is shown in Fig. 1b3. The powdery sample typically demonstrated improved diffraction peak signal, showing a series of diffraction peaks that confirm the existence of monoclinic crystalline CuO. Notably, for both foil samples, the existence of metallic Cu can be verified, again confirming limited thermal oxidation of the Cu substrate in our synthetic conditions, guaranteeing good conductivity and flexibility for subsequent usage. Also, no diffraction peaks can be attributed to Cu_2O or $Cu(OH)_2$ for both the foil and powdery samples, determining the complete decomposition of $Cu(OH)_2$ and the purity of the CuO phase.

The microstructures of the $Cu(OH)_2$ and CuO NWs were characterized by field-emission scanning electron microscopy (FE-SEM) and transmission electron microscopy (TEM) as shown in Fig. 1c and d, respectively. As can be seen in Fig. 1c1, the surface of the copper foil is covered with large-area grass-like $Cu(OH)_2$ NW with high density and good uniformity. These vertical nanowires are in a radially protruding fashion as shown in Fig. 1c2. The further magnified view in Fig. 1c3 shows the axial straightness of the nanowires and the diameter

Published on 10 November 2014. Downloaded by Fail Open on 23/07/2025 9:15:02 AM.

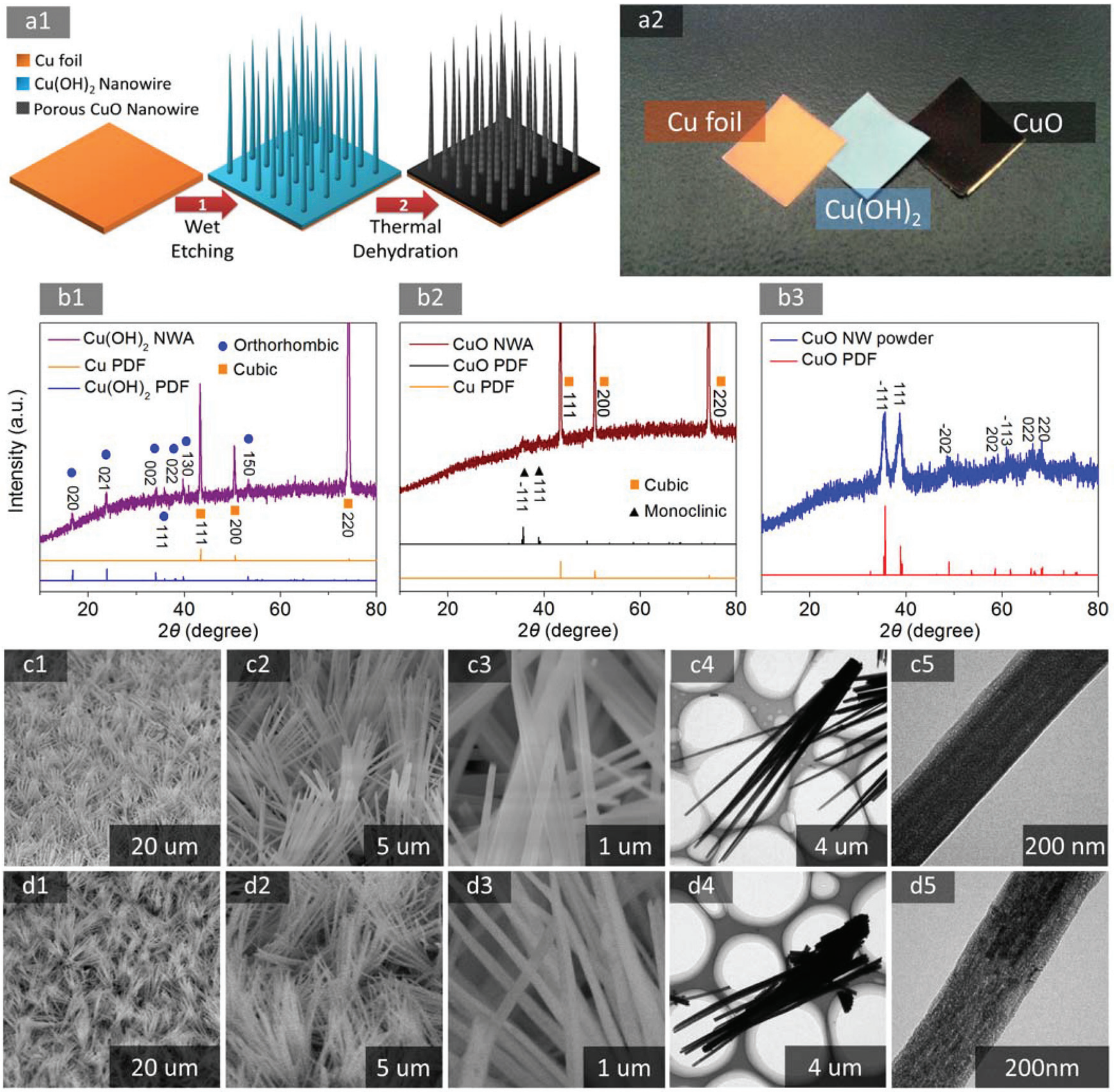

Fig. 1 (a1) Schematic illustration of synthesis of porous CuO NWA on copper foils; (a2) digital photograph of a primitive Cu foil and the foils covered with $Cu(OH)_2$ and CuO NWA; XRD patterns of $Cu(OH)_2$ NWA (b1), CuO NWA (b2) and CuO NW powders (b3); SEM images of $Cu(OH)_2$ NWA (c1 to c3) and CuO NWA (d1 to d3); TEM images of $Cu(OH)_2$ NW (c4 to c5) and CuO (d4 to d5) NWs.

is about 100–200 nm, with a tapering outline. Interestingly, the CuO NWs are arranged in a manner where several closely aligned nanowires share a common bundled end. This is further ascertained by TEM characterization shown in Fig. 1c4. In accordance to the SEM characterization, the closely grown $Cu(OH)_2$ NWs have a common connection at their 'roots', which was so firm that it remained undamaged after ultrasonication during the TEM sample preparation. The nanowires are about 10 μm in length, which can also be estimated in the SEM images. Fig. 1c5 offers a close-up view of a single $Cu(OH)_2$ NW. The surface of the nanowire is generally smooth with a slightly discernible sign of the existence of a porous outer shell, possibly owing to the instability of $Cu(OH)_2$ under the high-energy electron beam impact in TEM characterization, which leads to partial decomposition.[38] All these results demonstrate the successful *in situ* preparation of vertical $Cu(OH)_2$ NWA using the mild wet chemical etching protocol. This method towards aligned NWA requires no templates,[25,39] shape-directing agent,[40] noble metal intermediates[41] or pre-seeding on substrates,[13,42] making it a facile choice that is potentially promising for scaled-up production. Moreover, the acid-removable nature of $Cu(OH)_2$ implies that this protocol can be possibly extended to synthesize other functional NWA structures with the $Cu(OH)_2$ NWA as a sacrificial template.[18] The formation of the $Cu(OH)_2$ NWA resulted from the interaction between the Cu species and the etchant in the AOES. Specifically, as the oxidative $S_2O_8^{2-}$ attacks Cu at the foil surface, $Cu^{(0)}$ is oxidized to $Cu^{(II)}$ and dissolved as ions into the solution. Instead of diffusing away, the $Cu^{(II)}$ interacts with OH^- and constructs itself in a manner similar to self-assembly. The high pH (>14) milieu subsequently leads to evolution of corrugated layers of $Cu(OH)_2$, which grows by olation

Published on 10 November 2014. Downloaded by Fail Open on 23/07/2025 9:15:02 AM.

reaction of Cu^{2+} and OH^- preferentially along the [100] direction because of the shortest inter-planar distance of (100) and the relatively stronger hydrogen bonding interaction.[36] In this dissolution and bottom-up way, the one-dimensional morphology is thus formed.

Successful transformation from $Cu(OH)_2$ to CuO is unambiguously demonstrated in the XRD patterns as was discussed. The SEM images in Fig. 1d1 to d3 present the as-prepared CuO NWA at various magnifications, from which no significant variance of the NWA morphology is observed. This is possibly due to the controlled heating rate in the annealing procedure that prevented fierce H_2O vapor departure in the dehydration reaction, which may threaten to cause rupture of the nanowires. Fig. 1d4 presents a TEM image of the CuO NWs, where it is found that the nanowires are slightly shorter than their $Cu(OH)_2$ precursor. In addition, as we observed the sample using TEM, we found more small broken pieces of nanowire in the case of CuO than of $Cu(OH)_2$, which suggested intensified breakage of the CuO NWs during ultrasonication for sample preparation. A close-up examination of a CuO NW is presented in Fig. 1d5. Compared to the $Cu(OH)_2$ NW in Fig. 1c5, porosity in CuO NW is more evident, which is perceptible not only at the outer shell. Further magnified TEM images in Fig. S1† reveal that CuO NW is composed of closely interconnected small CuO particles with pores and gaps in between. The porous structure was further characterized by nitrogen sorption isotherms that present typical type-IV isotherms and the pore size distribution determined from the adsorption branch with the Barrett–Joyner–Halenda (BJH) method are shown in Fig. S3.† Apparently, dehydration reaction caused breakage of the $Cu(OH)_2$ NW bulk into smaller CuO particles that remained in touch with each other and preserved the overall 1D morphology. This should answer for the aggravated susceptibility to ultrasonication since the CuO NWs with increased porosity have weakened mechanical strength along its high aspect-ratio axial direction compared to the $Cu(OH)_2$ counterpart. Despite this, the porous profile which provides further increased surface area may be favorable for electrochemical sensing applications. Understandably, the porosity evolved during dehydration where H_2O vapor evaporated out and left pores in the nanowire bulk. This mechanism of generation of pores, which is unique from those reported protocols engaging sacrificial templates,[43] pore-forming agents,[44] and electrochemical ion insertion,[45] possibly offers a general and facile approach for porous metal oxide nanostructures from the corresponding hydroxide precursors to be further explored.

Enzymeless sensing of glucose

Efficient utilization of nano-sized electrocatalysts as building blocks to construct high-performance sensor electrodes remains challenging. Electrode construction techniques and electrode architectures of catalytic materials can exert considerable influence on the performance. Herein, with the *in situ* prepared CuO NWA, we carried out proof-of-concept research to study the performance of the two most representative nanowire architectures for amperometric sensing of glucose.

Firstly, two types of electrodes were prepared. One featured vertical nanowire array electrode architecture (denoted as NWA) while the other was fabricated by conventional modification protocol, with CuO NWs piled (denoted as NWP) randomly in Nafion film that was drop casted on a glassy carbon electrode (GCE). Its microscopic image is shown in Fig. S2,† while the microstructure of the working portion of the NWA electrode is considered the same as the freshly prepared samples. For both electrodes, the weight of the CuO NW per geometric surface area ($W_{(\mathrm{CuO})}/S_{(\mathrm{geo})}$) was kept identical. The details and fabrication flowchart (Fig. S3†) can be found in the Experimental section and ESI,† respectively. To collect information on the electrocatalytic ability of the CuO NW-based electrodes towards glucose electro-oxidation, evaluation by means of cyclic voltammetry (CV) was first performed (Fig. 2). For the NWA electrode, when glucose is absent, no typical oxidation peak can be observed in the positive scan from 0 V to 0.8 V (Fig. 2a). With increased concentration of glucose, an oxidation peak around 0.35 V appeared. For the reverse scan from 0.8 V to 0 V, the cathodic current experienced a gradual decrease as the glucose concentration increased. These observations typically indicate an irreversible electro-oxidation process of glucose. In Fig. 2b, the CV curves of a primitive planar Cu electrode (PCE) are presented in comparison with the CuO NWA. As can be clearly seen, the PCE can also electro-oxidize glucose, with increased anodic current peaking at 0.51 V and the turn-on potential is situated at around 0.36 V. Both positively shifted potential parameters suggest the sluggish electro-oxidation kinetics of the PCE compared to the CuO NWA, whose turn-on potential was as low as 0.18 V. Peaking current density is also far higher for the NWA. The facilitated electrocatalytic oxidation of glucose from the CuO NWA is unequivocally derived from the cooperative effect of the electroactive CuO and nanoengineered NWA structure. Also, it is noted for the blank sample (without glucose) that the CuO NWA exhibits much higher current density than the primitive Cu foil planar electrode, suggesting significantly increased surface area, surface energy and boosted electron transfer from the vertically protruding porous CuO NWs.[8] The CV data of the CuO NWP electrode was also recorded. It is not surprising that the NWP electrode was able to carry out the irreversible electro-oxidation process (Fig. 2e) analogous to the NWA one. Since there is no typical signal corresponding to electro-oxidation of glucose at a bare GCE (Fig. 2f), the electrocatalytic effect of the NWP electrode is undoubtedly attributed to the CuO NWs. Notably, *ex situ* introduction of CuO NWs also leads to significantly amplified background current compared to the bare GCE, which exemplifies the advantage of nanostructured electrodes in enhancing electrode–electrolyte interactions. Taking all these into account, the feasibility of using the as-prepared CuO NW for enzymeless glucose sensing is preliminarily confirmed. The electro-oxidation process at the two electrodes was further explored by CV at different scan rates ranging from 10–100 mV s^{-1}, as shown in Fig. 2c and g, and the relationship linearly fitted in Fig. 2d and h suggests the surface adsorption-controlled nature of the electrocatalytic

This journal is © The Royal Society of Chemistry 2015

Published on 10 November 2014. Downloaded by Fail Open on 23/07/2025 9:15:02 AM.

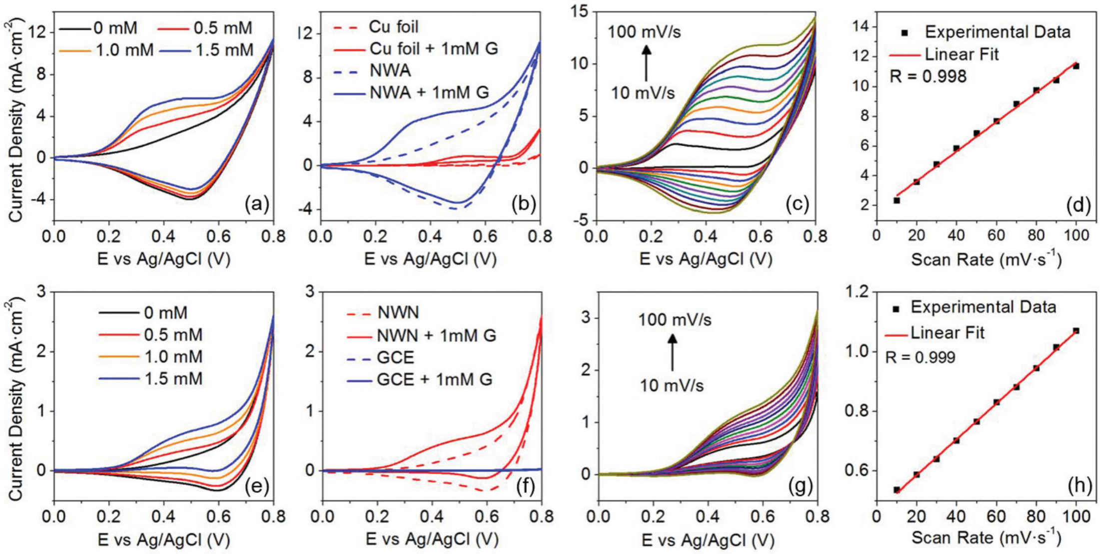

Fig. 2 CV profiles with different concentrations of glucose of (a) CuO NWA and (e) CuO NWP; CV with glucose in absence and presence of (b) CuO NWA compared with planar Cu electrode and (f) CuO NWP compared with GCE; CV at scan rates from 10 to 100 mV s^{-1} for (c) CuO NWA and (g) CuO NWP in 2.5 mM glucose. (d) The calibration plot of (c). (h) The calibration plot of (g).

process. While the explicit mechanism for CuO-catalyzed electro-oxidation of glucose in alkaline has not been completely settled, the generally accepted proposal suggests the formation of a high valence Cu^{III} intermediate that readily oxidizes glucose into gluconic acid,[3,5] which can be described with the following reactions:

$$CuO + 2OH^- + H_2O \rightarrow Cu(OH)_4{}^- + e^- \text{or } CuO + OH^- \rightarrow CuOOH + e^-$$

$$Cu^{III} + \text{glucose} \rightarrow Cu^{II} + \text{gluconic acid}$$

Accordingly, the mechanism for electrochemical sensing of glucose by the NWA and NWP electrodes is depicted in Fig. 3. Cu^{II} is electro-oxidized to Cu^{III}, which is a highly oxidative species and subsequently interacts the adsorbed glucose at the nanowire surface, oxidizes it into gluconic acid and is then reduced to the original Cu^{II}. Upon this cycling, electrons generated from the electro-oxidation of Cu^{II} transport through the nanowire to the underlying conductive substrate, generating the anodic signal.

Amperometric *i*–*t* analysis was carried out to deduce the linear relationship between the analyte concentration and

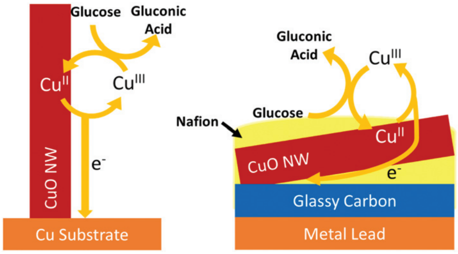

Fig. 3 Mechanism of the electro-oxidation of glucose at the CuO NW-based electrodes.

current responses of the NWA and NWP electrodes, with their respective peaking potentials applied during the tests. Generally, both of them give stair-like *i*–*t* curves under stepwise addition of glucose, with the low-concentration parts magnified in the respective insets, as shown in Fig. 4a and b. Upon the test, after the current reached a steady state, a predetermined amount of glucose was successively injected into the magnetically stirred solution, which immediately induced leaping of the current. The rapidness of the signal response of the CuO NWA was confirmed by observation of the magnified amperometric curves (Fig. S4†), which show 90% current change was completed in about 1 s and current plateaus were generally achieved in 2 s within the linear range. This fast current response is a benefit of the high surface area 1D morphology and the open spaces in the nanowire array structure that allow adequate interfacing with the solution phase and facilitated diffusion of analyte molecules. The NWP also offered comparably quick current feedback. When the analyte concentration reached a certain level, the amperometric signal became saturated. The concentration–signal relationship is plotted in Fig. 4c. Note that for comparison, the *i*–*t* performance of the NWP electrode under 0.35 V (the working potential used for the NWA electrode) was also recorded (Fig. S5†). The calibration equations deduced from linear regression of the experimental data for the NWA (1), NWP under 0.45 V (2) and 0.35 V (3) are as listed below:

$$J\ (\text{mA cm}^{-2}) = 1.42034\ C\ (\text{mM}) + 0.11254 \quad (1)$$

$$J\ (\text{mA cm}^{-2}) = 0.25012\ C\ (\text{mM}) + 0.01707 \quad (2)$$

$$J\ (\text{mA cm}^{-2}) = 0.19712\ C\ (\text{mM}) + 0.00359 \quad (3)$$

where J and C stand for current density and analyte concentration, respectively. As fitted, the CuO NWA demonstrated an

Published on 10 November 2014. Downloaded by Fail Open on 23/07/2025 9:15:02 AM.

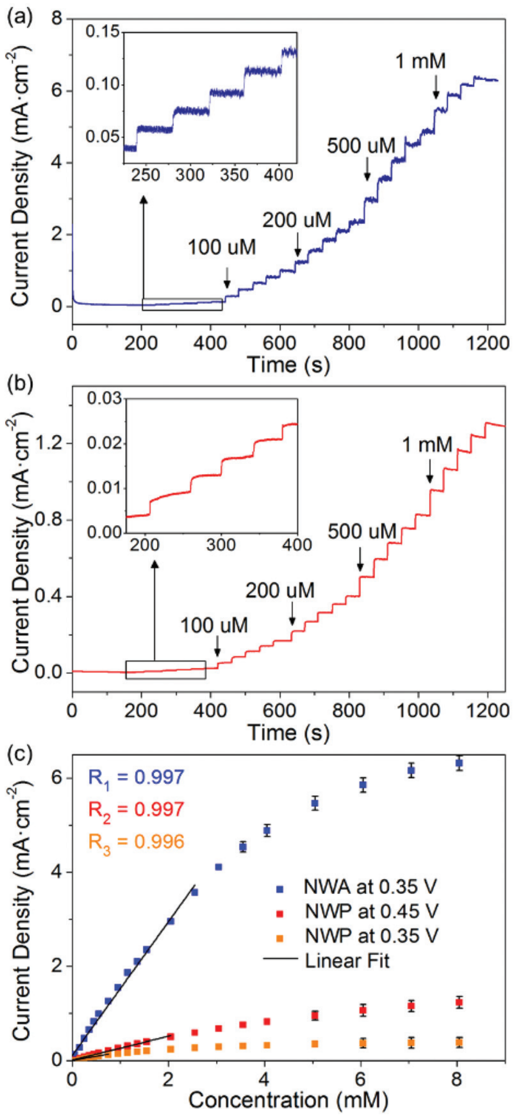

Fig. 4 Amperometric *i*–*t* test with successive addition of glucose for the NWA under +0.35 V (a) and the NWP under +0.45 V (b). (c) Calibration plots of (a) and (b). The insets show respective *i*–*t* curves at low concentration levels, with stepwise addition of 10 μM glucose.

excellent sensitivity of 1420.3 μA cm^{-2} mM^{-1} with a linear range up to ~2.55 mM and a detection limit of 5.1 μM (3 signal-noise ratio). The CuO NWP exhibited a sensitivity of 250.1 μA cm^{-2} mM^{-1}, a linear range up to ~2.05 mM and a detection limit of 1.9 μM, under the applied potential of 0.45 V. For its counterpart under 0.35 V, the corresponding performance parameters are determined to be 197.1 μA cm^{-2} mM^{-1} (sensitivity), ~0.75 mM (linear range) and 0.7 μM (detection limit). Obviously, among the three cases, the NWA presents a much higher sensitivity than the other two. When the applied potential was the same (0.35 V), the sensitivity of the NWA is 7 times that of the NWP. When the working potential was optimized at the respective peaking potentials, the NWA still shows a sensitivity above 5 times higher than the NWP despite working at a lower (by 100 mV) potential. In addition to its outperforming performance over the NWP electrode in this work, the overpotential for the CuO NWA to carry out sensing functionality is also smaller than most CuO-based glucose sensors,[8,17,46–50] and the sensitivity exceeds many *ex situ* immobilized 1D CuO-based enzymeless glucose sensors, as listed for comparison in Table S1.†

While the NWA and NWP electrodes have both shown improved electrochemistry compared with the primitive PCE and bare GCE, the former obviously overshadowed the latter. As the apparent $W_{(\mathrm{CuO})}/A_{(\mathrm{geo})}$ of the electrocatalyst was pre-controlled, the possibility of the amount of active material being a main cause of performance difference can be ruled out. The positive sweeping of the CV of the electrocatalytic reaction on which the sensing functionality is based has been studied, as shown in Fig. 5a. In addition to the aforementioned higher anodic peak potential (by ~100 mV) of the NWP, the reaction turn-on potential of the NWP (0.23 V) is also positively shifted by about 50 mV compared with the NWA. Obviously a higher overpotential is required for the NWP. Furthermore, the current magnitude of the NWA is also much larger than the NWP. We first sought to consider these phenomena from the view of activity degradation of CuO in the NWP electrode. Actually, this is hardly possible because the sensor fabrication procedures induced no force powerful enough to chemically change the stable CuO. Besides, the Tafel plot in Fig. 5b also reveals that the NWA and NWP have very close Tafel slopes, 163 mV dec^{-1} for the NWP and 169 mV dec^{-1} for the NWA. Since the Tafel slope is related to the activation energy of a certain electrochemical reaction, this denies change of catalytic

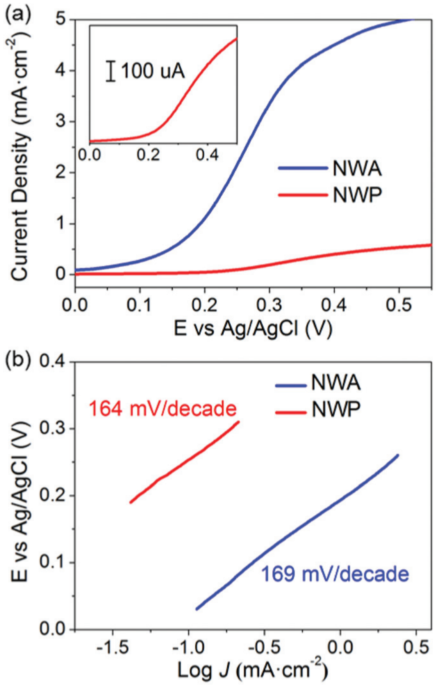

Fig. 5 (a) Positive scanning of CV measurements in the presence of 1 mM glucose; inset shows the magnified curve for the NWP. (b) The corresponding Tafel plot of (a).

This journal is © The Royal Society of Chemistry 2015

Published on 10 November 2014. Downloaded by Fail Open on 23/07/2025 9:15:02 AM.

ability as a determining factor that brought about the varied performances.

Therefore, the performance difference must be connected to the overall electrode architecture. Due to the inherent structure of the modifying film in the NWP electrode, disorderly stacking style can result in a portion of nanowires that failed to gain direct contact to the conductive GC, which resembles a film of stacking nanoparticles where defined charge transport pathway is absent and electrons have to go through multiple interfaces. Both aspects weaken the positive effect of CuO NWs in shuttling electrons between the analyte and the current collector. As a consequence of the increased interfacial resistance, the overall series resistance becomes larger, which can be determined using electrochemical impedance spectroscopy (EIS). Both the NWA and NWP electrodes feature a reaction-controlled part (semicircle) at frequencies and a diffusion-controlled part (oblique line) at low frequencies in their Nyquist plots (Fig. S6†). As the diameter of the semicircle reflects the electron transfer resistance, R_{et}, it can be found that R_{et} of the NWA is much smaller compared to the NWP electrode, in accordance with the performance and analysis, implying better electron transfer.[51,52] Also, as we characterized CuO NWP-Nafion film (Fig. S7†), it was found that isolation of fractured CuO NWs may occur, namely nano-sized CuO was isolated within/on the polymer matrix without contact with other CuO NWs or the conducting GC. This can be aggravated when the ultrasonication, although important for forming homogeneous casting suspension, led to more low-aspect-ratio CuO particles from the mechanical fracture of the CuO NWs. Such isolated CuO and those blocked by Nafion polymer binder cannot engage in electrocatalysis by failing as an electrochemically active bridge between the analyte and the GC. In contrast, both good electron transport between the catalytic units and the external circuit, and abundance of electrochemically connected and analyte-accessible active sites exist in the NWA electrode, which favors the sensing platform making full use of the active CuO.

In further exploring the CuO NWA as a reliable platform for enzymeless glucose sensing, practical testing conditions need to be taken into consideration. In real samples, co-existing electroactive species with comparable reducibility such as ascorbic acid (AA), uric acid (UA) and other reducing sugars with similar chemical structures may cause unwanted interference. The relatively high concentration (~100 mM) of Cl^- in blood, which was reported to poison some metal-based sensors, must also be considered. To find out whether the selectivity of the sensor is good enough to preclude interference from the mentioned species and its poisoning-proof ability against Cl^-, we further conducted amperometric *i*–*t* test with different interfering species successively added and the supporting electrolyte containing 0.2 M NaCl. The concentration of the interfering species was fixed 1/10 of the glucose despite their actually lower ratio (1/40 to 1/30) to glucose in human blood.[53] As shown in Fig. 6a, the steady current

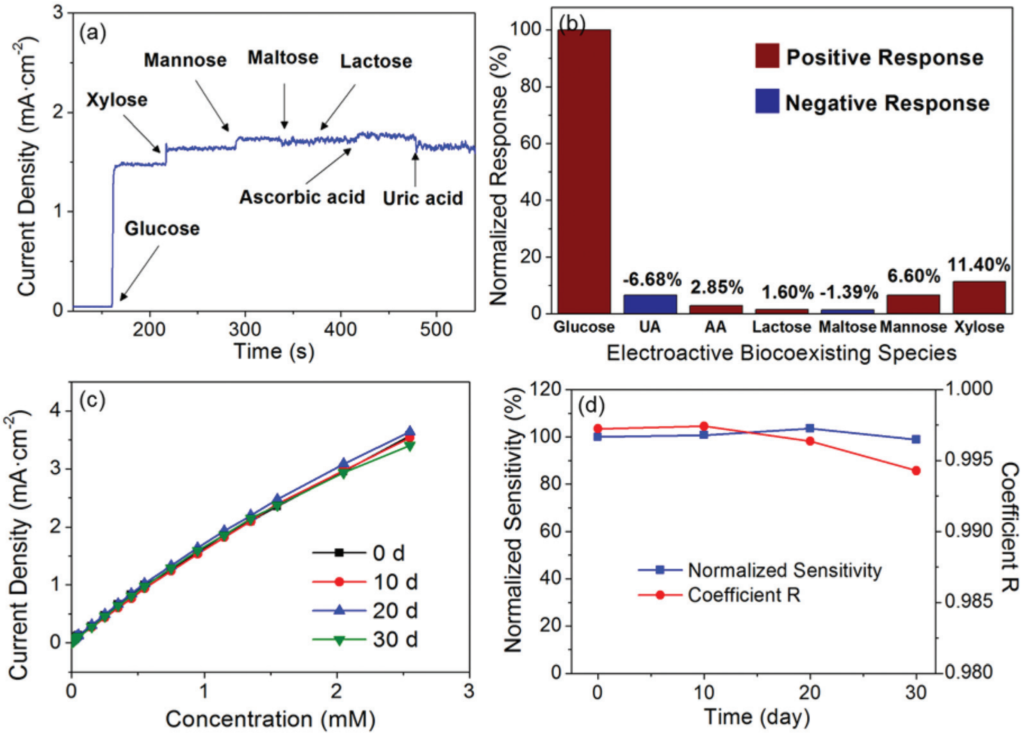

Fig. 6 (a) Amperometric test for selectivity and anti-Cl^--poisoning of the NWA sensor and (b) percentage of interfering signals to the target analyte. (c) Calibration plots within the linear range and (d) normalized sensitivity and the corresponding Pearson coefficients of the CuO NWA sensor after different days.

Published on 10 November 2014. Downloaded by Fail Open on 23/07/2025 9:15:02 AM.

experienced a significant increase as 1 mM glucose was added at the experimental runtime of 160 s. In contrast, only moderate current responses were observed when the interfering species including xylose, mannose, maltose, lactose, AA and UA were successively added. Interfering signals were −6.68%, 2.85%, 1.60%, −1.39%, 6.60% and 11.40% for the respective species (Fig. 6b), which were all acceptable. What is more, despite the high concentration of Cl^- present, the sensor's response was not degraded. A further recovery test was performed to demonstrate its reliability (Fig. S9†), where blood glucose mimic liquid (LifeScan, Inc.) with pre-determined concentration was injected twice into the electrolyte followed by two-time injection of 20 μM standard concentration of glucose. The results of the recovery test tabulated in Table S2† shows the respective recovery of 95% and 98%, and the relative deviation of the found concentrations for blood glucose mimic liquid from the commercially calibrated value is less than 6%. The long-run stability of the CuO NWA sensor was also evaluated by testing its performance after having left the NWA electrode in ambient condition without special protection for 10, 20 and 30 days. The absolute current responses (Fig. 6c) showed no dramatic change. Besides, neither the sensitivity and linear relevancy (Fig. 6d) experienced great variance. A slight decrease of sensitivity by less than 2% over a period of 30 days is much lower than the data reported in a series of literature on enzymeless glucose sensors.[49–51,54,55] This splendid retention of sensitivity could be attributed to the synergistic effect of the stable chemical property of CuO and the exceptional flake-off resistance of the *in situ* grown NWA structure.

Flexible CuO NWA as bendable sensor electrode

The advantage of *in situ* grown NWA on thin conductive substrate comes not only from the superior performance demonstrated above, but also from its compatibility to further integration into flexible devices. In Fig. 7a, a small foil slice of CuO NWA is shown being directly bent by hand. Endowing flexibility to electrodes is gaining growing preference due to the light weight, durability, user convenience, and feasibility for rolled-up production therefore acquired.[56] Consequently, an archetypal flexible sensor (Fig. 7b) was constructed. The reliability of the sensing performance against mechanical input was assessed by amperometry. First, the exposed area (3.5 cm × 0.6 cm) with CuO NWA was bent with the curvature radii (ρ) fixed at 18.5 and 11.5 mm (Fig. 7c) and the i–t responses to analyte addition are shown in Fig. 7e. At the moderate curvature ($1/\rho = 0.0541\ \text{mm}^{-1}$, $\rho = 18.5$ mm), the current response towards 10, 50 and 100 μM glucose showed negligible deviation from what was measured in the unbent condition ($1/\rho = 0$, $\rho = \infty$). Even when it reached a high curvature ($1/\rho = 0.0870\ \text{mm}^{-1}$, $\rho = 11.5$ mm), the sensitivity remained 90% relative to the flat state. This proves that the sensor has eligible performance stability against bending. To further explore its capability against mechanical fatigue, the sensor was mounted onto a home-made tester and the CuO NWA portion was repeatedly bent and relaxed. Fig. 7d displays the sensor under flat (upper) and maximum bending (lower) conditions. The CuO NWA portion got bent as the clamp moved left. After the maximum travel distance of 10 mm was completed, the clamp moved right until the bent CuO NWA returned to its original state. This bending-relaxation process made up one cycle. After 10, 100, and 1000 cycles, respective amperometric tests were performed. The current curves in Fig. 7f clearly demonstrate that the sensor exhibits robust performance reliability against long-run mechanical input, with insignificant departure from the flat condition after 100 cycles. Although discernible response degradation was observed after 1000 cycles, performance conservation as high as 90% of the initial amperometric response was quite satisfactory. These results indicate that the flexible CuO NWA has promise to be further engineered and optimized to construct flexible sensing devices with high sensitivity, rapid response and robust durability.

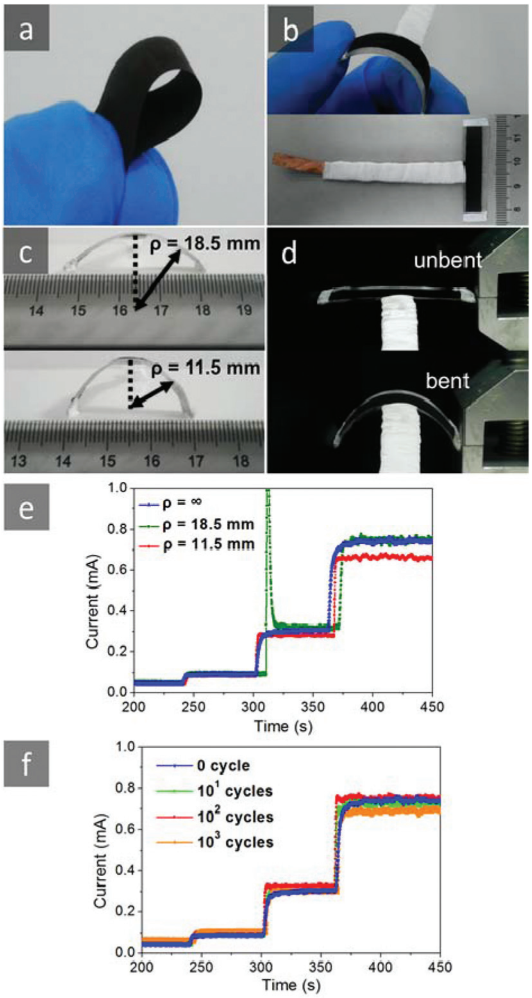

Fig. 7 (a) A flexible slice of CuO NWA; (b) flexible sensor under its bent (upper) and unbent (lower) conditions; (c) flexible sensor bent with curvature radii of 18.5 mm (upper) and 11.5 mm (lower); and (d) bending-relaxation tests showing the sensor unbent (upper) and maximum bent (lower). Current response at different curvature radii (e) and after different bending-relaxation cycles (f) to addition of 10, 50 and 100 μM glucose.

This journal is © The Royal Society of Chemistry 2015

Published on 10 November 2014. Downloaded by Fail Open on 23/07/2025 9:15:02 AM.

Experimental

Synthesis of CuO NWA

The synthetic procedure involved solution-processed etching of copper foils and dehydration of the thus-obtained $Cu(OH)_2$ NWA. Typically, AOES was prepared by dissolving 0.913 g $(NH_4)_2S_2O_8$ in 22 mL of deionized water and dropwise addition of 8 mL of freshly prepared 10 M NaOH into the $(NH_4)_2S_2O_8$ solution under moderate stirring. After the AOES cooled to room temperature, its pH (>14) was confirmed. Cleaned with diluted HCl and successively ultrasonicated in acetone and ethanol, the copper foils (X%) were rinsed using deionized water and immediately immersed in the AOES. When the surface of the copper foils turned light blue, they were taken out of the solution, thoroughly rinsed with deionized water and dried in air. Then the samples went through four-hour dehydration under 180 °C in air at a ramp rate of 2 °C min^{-1}, and the color eventually turned to dark brown. The temperature was allowed to cool to room temperature gradually before opening the furnace.

Sensor fabrication

For the NWA electrode, preparation of CuO NWA on a copper foil was the same as formerly described except that the degreased copper foil may be pre-masked by a piece of scotch tape before being dipped in the AOES. Subsequently, the CuO NWA was mounted on a plastic substrate with its rear side and the bare copper part (acting as the lead) sealed by thermosetting insulating epoxy. For the CuO NWP electrode, the CuO NWs were carefully collected using the doctor-blade method and were dispersed in deionized water containing 0.5 wt% Nafion (Dupont). The concentration of the CuO NW was adjusted by the amount of solvent added so that every 10 μL of the suspension has the weight of CuO NW equivalent to the amount collected from 0.0707 cm^2 (the geometric surface area of the GCE, 3 mm in diameter) of CuO NWA foil. After a GCE was successively polished with alumina powders (1 and 0.05 μm), 10 μL of the suspension was drop-cast on the GCE, which was left to dry up naturally. For the archetypal flexible CuO NWA sensor, the starting copper foil was clipped into the desired shape for convenience in subsequent experiments. After the preparation of CuO NWA on the foil, the CuO NWA foil was firmly bound onto a tailored PET slice using soft double-sided adhesive tape, and both ends were further secured by Teflon tape. The pre-masked metallic copper area for external electrical connection was sealed off from contact with the electrolyte with epoxy resin and Teflon tape. The whole sensor electrode is T-shaped (Fig. 7b). Note that this shape was intentionally designed for facile operation of bending the CuO NWA part and can be further adjusted according to practical requirements.

Characterization

X-ray diffraction (XRD) characterization (40 kV, 100 mA) was performed on an X-ray diffractometer (D/MAX 2550, Rigaku) equipped with a RINT2000 vertical goniometer and a Cu Kα radiation generator. Microscopic analysis of foil samples and drop-cast CuO NW-Nafion film was carried out using field-emission scanning electron microscopy (FE-SEM, S-4800, Hitachi) at an accelerating voltage of 15.0 kV and emission current of 10 μA. Micrographs of scratched nanowires were taken using transmission electron microscopy (TEM, JEM 2011, JEOL). Electrochemical measurements including cyclic voltammetry (CV), amperometric *i–t* tests and electrochemical impedance spectroscopy (EIS) were carried out with an electrochemical workstation (CHI660c, Shanghai Chenhua Co.) under conventional three-electrode configuration, employing a Pt wire electrode and an Ag/AgCl electrode (KCl-saturated) as counter electrode and reference electrode, respectively. Working electrodes were different CuO NW-based electrodes or GCE electrodes modified with or without Nafion. 0.1 M NaOH supporting electrolyte and all standard analyte solutions were freshly prepared for all experiments. For all CV measurements, the scan rate was 50 mV s^{-1} unless otherwise mentioned. Amperometric *i–t* data were collected under fixed potential and magnetically stirred conditions. The standard analyte solution was injected after the current curve reached a steady baseline. EIS was performed at a frequency range of 10 kHz to 0.01 Hz with amplitude of 5 mV employing 5 mM $[Fe(CN)_6]^{3/4-}$ in 0.1 M KCl as the redox probe.

Conclusions

In situ synthesis of CuO NWA on a conductive substrate has been realized and XRD, SEM and TEM were applied to confirm its structure and components. In addition to the extraordinary sensitivity and stability for enzymeless sensing functionality, with the *in situ* formed 3D array structure and intact connection to the underlying conducting substrate, the CuO NWA showed obviously enhanced electrode kinetics for glucose electro-oxidation and outperforming sensitivity over its counterpart of freely stacked CuO NWP entrapped within the polymer binder prepared by conventional casting, which suggests that the large-scale arrangement of nanowire electrocatalyst and the electrode architecture are crucial to efficiently realizing the sensing functionality of electroactive CuO NWs. The CuO NWA also showed compatibility for construction of a flexible sensing platform, which can give satisfyingly stable performance under and after mechanical bending. Benefiting from its *in situ* growth style and high-density vertical structure, as well as the multifunctionality offered by CuO, it can be inferred that the CuO NWA may become a useful tool for determining other bio-analytes, and can also be a potential candidate in other electrochemical applications, such as energy storage and conversion, *etc*.

Acknowledgements

This work was supported by the National Natural Science Foundation of China (21471056, 21236003, 21206042, and

21176083), the Basic Research Program of Shanghai (13NM1400700, 13NM1400701), and the Fundamental Research Funds for the Central Universities.

Published on 10 November 2014. Downloaded by Fail Open on 23/07/2025 9:15:02 AM.

Notes and references

1 A. Heller and B. Feldman, *Chem. Rev.*, 2008, **108**, 2482.
2 J. Wang, *Chem. Rev.*, 2008, **108**, 814.
3 S. K. Meher and G. R. Rao, *Nanoscale*, 2013, **5**, 2089.
4 C. Chen, Q. Xie, D. Yang, H. Xiao, Y. Fu, Y. Tan and S. Yao, *RSC Adv.*, 2013, **3**, 4473.
5 G. Wang, X. He, L. Wang, A. Gu, Y. Huang, B. Fang, B. Geng and X. Zhang, *Microchim. Acta*, 2013, **180**, 161.
6 S. Park, H. Boo and T. D. Chung, *Anal. Chim. Acta*, 2006, **556**, 46.
7 J. Chen, W. D. Zhang and J. S. Ye, *Electrochem. Commun.*, 2008, **10**, 1268.
8 E. Reitz, W. Jia, M. Gentile, Y. Wang and Y. Lei, *Electroanalysis*, 2008, **20**, 2482.
9 J. Huang, Y. Zhu, H. Zhong, X. Yang and C. Li, *ACS Appl. Mater. Interfaces*, 2014, **6**, 7055.
10 S. Su, X. Wei, Y. Guo, Y. Zhong, Y. Su, Q. Huang, C. Fan and Y. He, *Part. Part. Syst. Charact.*, 2013, **30**, 326.
11 C.-J. Zhong, J. Luo, P. N. Njoki, D. Mott, B. Wanjala, R. Loukrakpam, S. Lim, L. Wang, B. Fang and Z. Xu, *Energy Environ. Sci.*, 2008, **1**, 454.
12 H. Tüysüz, Y. J. Hwang, S. B. Khan, A. M. Asiri and P. Yang, *Nano Res.*, 2013, **6**, 47.
13 Z. Yin, Z. Wang, Y. Du, X. Qi, Y. Huang, C. Xue and H. Zhang, *Adv. Mater.*, 2012, **24**, 5374.
14 B. Liu, X. Wang, H. Chen, Z. Wang, D. Chen, Y. B. Cheng, C. Zhou and G. Shen, *Sci. Rep.*, 2013, DOI: 10.1038/srep01622.
15 X. Zhang, W. Shi, J. Zhu, D. J. Kharistal, W. Zhao, B. S. Lalia, H. H. Hng and Q. Yan, *ACS Nano*, 2011, **5**, 2013.
16 W. Jia, M. Guo, Z. Zheng, T. Yu, Y. Wang, E. G. Rodriguez and Y. Lei, *Electroanalysis*, 2008, **20**, 2153.
17 H. Wu, S. Zhou, Y. Wu and W. Song, *J. Mater. Chem. A*, 2013, **1**, 14198.
18 M. A. Lim, D. H. Kim, C. O. Park, Y. W. Lee, S. W. Han, Z. Li, R. S. Williams and I. Park, *ACS Nano*, 2011, **6**, 598.
19 M. T. Mayer, C. Du and D. Wang, *J. Am. Chem. Soc.*, 2012, **134**, 12406.
20 A. Kim, Y. Won, K. Woo, C. H. Kim and J. Moon, *ACS Nano*, 2013, **7**, 1081.
21 M. D. Kelzenberg, S. W. Boettcher, J. A. Petykiewicz, D. B. Turner-Evans, M. C. Putnam, E. L. Warren, J. M. Spurgeon, R. M. Briggs, N. S. Lewis and H. A. Atwater, *Nat. Mater.*, 2010, **9**, 239.
22 Q. Li, P. Xu, B. Zhang, H. Tsai, S. Zheng, G. Wu and H.-L. Wang, *J. Phys. Chem. C*, 2013, **117**, 13872.
23 X. Zhang, H. Yin, J. Wang, L. Chang, Y. Gao, W. Liu and Z. Tang, *Nanoscale*, 2013, **5**, 8392.
24 D. Pradhan, F. Niroui and K. T. Leung, *ACS Appl. Mater. Interfaces*, 2010, **2**, 2409.
25 M. Jamal, M. Hasan, A. Mathewson and K. M. Razeeb, *Biosens. Bioelectron.*, 2013, **40**, 213.
26 Y. Zhang, Y. Liu, L. Su, Z. Zhang, D. Huo, C. Hou and Y. Lei, *Sens. Actuators, B*, 2014, **191**, 86.
27 M. S. Hsu, Y. L. Chen, C. Y. Lee and H. T. Chiu, *ACS Appl. Mater. Interfaces*, 2012, **4**, 5570.
28 P. Si, S. Ding, J. Yuan, X. W. Lou and D. H. Kim, *ACS Nano*, 2011, **5**, 7617.
29 L. Wang, X. Gao, L. Jin, Q. Wu, Z. Chen and X. Lin, *Sens. Actuators, B*, 2013, **176**, 9.
30 G. Wang, X. Lu, T. Zhai, Y. Ling, H. Wang, Y. Tong and Y. Li, *Nanoscale*, 2012, **4**, 3123.
31 R. Ahmad, N. Tripathy and Y. B. Hahn, *Chem. Commun.*, 2014, **50**, 1890.
32 B. Fang, C. Zhang, W. Zhang and G. Wang, *Electrochim. Acta*, 2009, **55**, 178.
33 X. Jiang, T. Herricks and Y. Xia, *Nano Lett.*, 2002, **2**, 1333.
34 A. Kargar, Y. Jing, S. J. Kim, C. T. Riley, X. Pan and D. Wang, *ACS Nano*, 2013, **7**, 11112.
35 Y. S. Kim, I. S. Hwang, S. J. Kim, C. Y. Lee and J. H. Lee, *Sens. Actuators, B*, 2008, **135**, 298.
36 W. Zhang, X. Wen and S. Yang, *Inorg. Chem.*, 2003, **42**, 5005.
37 W. Zhang, S. Ding, Z. Yang, A. Liu, Y. Qian, S. Tang and S. Yang, *J. Cryst. Growth*, 2006, **291**, 479.
38 W. Zhang, X. Wen, S. Yang, Y. Berta and Z. L. Wang, *Adv. Mater.*, 2003, **15**, 822.
39 H. Zhou and S. S. Wong, *ACS Nano*, 2008, **2**, 944.
40 A. I. Hochbaum, R. Fan, R. He and P. Yang, *Nano Lett.*, 2005, **5**, 457.
41 K. Q. Peng, J. J. Hu, Y. J. Yan, Y. Wu, H. Fang, Y. Xu, S.-T. Lee and J. Zhu, *J. Adv. Funct. Mater.*, 2006, **16**, 387.
42 G. Wang, Y. Wei, W. Zhang, X. Zhang, B. Fang and Z. L. Wang, *Microchim. Acta*, 2010, **168**, 87.
43 E. J. W. Crossland, N. Noel, V. Sivaram, T. Leijtens, J. A. Alexander-Webber and H. J. Snaith, *Nature*, 2013, **495**, 215.
44 A. Jain, V. Aravindan, S. Jayaraman, P. S. Kumar, R. Balasubramanian, S. Ramakrishna, S. Madhavi and M. P. Srinivasan, *Sci. Rep.*, 2013, DOI: 10.1038/srep03002.
45 Y. S. Hu, Y. G. Guo, W. Sigle, S. Hore, P. Balaya and J. Maier, *Nat. Mater.*, 2006, **5**, 713.
46 C. Kong, L. Tang, X. Zhang, S. Sun, S. Yang, X. Song and Z. Yang, *J. Mater. Chem. A*, 2014, **2**, 7306.
47 T. Soejima, H. Yagyu, N. Kimizuka and S. Ito, *RSC Adv.*, 2011, **1**, 187.
48 W. Wang, L. Zhang, S. Tong, X. Li and W. Song, *Biosens. Bioelectron.*, 2009, **25**, 708.
49 L. Luo, L. Zhu and Z. Wang, *Bioelectrochemistry*, 2013, **88**, 156.
50 J. Song, L. Xu, C. Zhou, R. Xing, Q. Dai, D. Liu and H. Song, *ACS Appl. Mater. Interfaces*, 2013, **5**, 12928.

This journal is © The Royal Society of Chemistry 2015

Published on 10 November 2014. Downloaded by Fail Open on 23/07/2025 9:15:02 AM.

51 H. Gao, F. Xiao, C. B. Ching and H. Duan, *ACS Appl. Mater. Interfaces*, 2011, **3**, 3049.

52 L. Kong, Z. Ren, S. Du, J. Wu and H. Fu, *Chem. Commun.*, 2014, **50**, 4921–4923.

53 Y. Ding, Y. Wang, L. Su, M. Bellagamba, H. Zhang and Y. Lei, *Biosens. Bioelectron.*, 2010, **26**, 542.

54 A. A. Ensafi, M. Jafari-Asl, N. Dorostkar, M. V. Ghiaci and J. L. G. Fierro, *J. Mater. Chem. B*, 2014, **2**, 706.

55 B. Fang, A. Gu, G. Wang, W. Wang, Y. Feng, C. Zhang and X. Zhang, *ACS Appl. Mater. Interfaces*, 2009, **1**, 2829.

56 M. Segev-Bar and H. Haick, *ACS Nano*, 2013, **7**, 8366.